Bulletin of the Seismological Society of America, Vol. 102, No. 1, pp. 64–72, February 2012, doi: 10.1785/0120110126

From Alarm-Based to Rate-Based Earthquake Forecast Models

by Peter Shebalin,* Clément Narteau, and Matthias Holschneider

Abstract We propose a conversion method from alarm-based to rate-based earthquake forecast models. A differential probability gain $g_{\text{alarm}}^{\text{ref}}$ is the absolute value of the local slope of the Molchan trajectory that evaluates the performance of the alarm-based model with respect to the chosen reference model. We consider that this differential probability gain is constant over time. Its value at each point of the testing region depends only on the alarm function value. The rate-based model is the product of the event rate of the reference model at this point multiplied by the corresponding differential probability gain. Thus, we increase or decrease the initial rates of the reference model according to the additional amount of information contained in the alarm-based model. Here, we apply this method to the Early Aftershock STatistics (EAST) model, an alarm-based model in which early aftershocks are used to identify space–time regions with a higher level of stress and, consequently, a higher seismogenic potential. The resulting rate-based model shows similar performance to the original alarm-based model for all ranges of earthquake magnitude in both retrospective and prospective tests. This conversion method offers the opportunity to perform all the standard evaluation tests of the earthquake testing centers on alarm-based models. In addition, we infer that it can also be used to consecutively combine independent forecast models and, with small modifications, seismic hazard maps with short- and medium-term forecasts.

Introduction

In statistical seismology, empirical and physical observations led to the development of two main types of numerical prediction experiments:

1. Alarm-based forecast models delimit the space–time region where an alarm function exceeds a given threshold value. In this region, an alarm is issued and a target earthquake with a magnitude $M \geq M_{\text{target}}$ is expected to occur. Exploring the entire range of threshold value from the highest to the lowest ones, the fraction of the space–time region occupied by alarms varies from 0 to 1.
2. Rate-based forecast models estimate for a given space–time region the rate parameter of the Poisson process that characterizes the occurrence of $M_{\text{min}} \leq M < M_{\text{max}}$ earthquakes. Most importantly for operational forecast, this rate may be converted into the probability of occurrence of an earthquake within the same magnitude range.

The conversion from rate- to alarm-based models is trivial because a sum of event rates on a given target-earthquake magnitude range can be considered as an alarm function. By contrast, there is actually no conversion method from alarm- to rate-based forecast models.

Using earthquake catalogs and observational constraints on fault slip rates, the number of earthquake predictability studies has increased significantly over the last five years, thanks to the activity of the Collaboratory for the Study of Earthquake Predictability (CSEP; Gerstenberger *et al.*, 2007; Jordan, 2006; Rhoades and Gerstenberger, 2009; Zechar and Jordan, 2010; Zechar, Schorlemmer, *et al.*, 2010). Nowadays, several CSEP testing centers operate worldwide to evaluate earthquake forecast models in different testing regions (Zechar *et al.*, 2007, Zechar, Gerstenberger, and Rhoades, 2010). In a vast majority of cases, these evaluations concern rate-based models with a time step of one day, three months, or five years, a testing region decomposed into a square grid of side length 0.1°, and a class interval of earthquake magnitude of 0.1 from $M \geq 3.95$ earthquakes. In parallel and for a longer term, several alarm-based models are being developed and tested by different groups. Known examples are the global and regional tests of M8, CN, and RTP (Keilis-Borok and Kossobokov, 1990; Keilis-Borok and Rotwain, 1990; Peresan *et al.*, 1999; Romashkova and Kossobokov, 2004; Shebalin *et al.*, 2004; Zechar, 2010). These algorithms are still difficult to adapt to all the CSEP evaluation methods because their alarm functions are not scaled to predicted event rates or probabilities. Hence, we present here a new method to convert alarm-based models into a form compatible with the requirements of all the CSEP testing centers.

*Also at the Institut de Physique du Globe de Paris, Sorbonne Paris Cité, Univ. Paris Diderot, UMR 7154 CNRS, 1 rue Jussieu, 75238 Paris, Cedex 05, France.

Our approach develops the concept of the probability gain G introduced by Gusev (1976) and Aki (1996). For an alarm-based model with a given threshold value of the alarm function, the G-value measures the ratio between the proportion of events predicted by this model and τ, the probability given by the reference model to observe an earthquake in the corresponding space–time region (Zechar *et al.*, 2007). More exactly, τ is the ratio of the earthquake frequency of the region occupied by alarms to the earthquake frequency of the entire space–time region. For a given target-earthquake magnitude, these rates are defined by the reference model. Interestingly, the G-value can also be directly estimated from the Molchan diagram that plots, for all threshold values of the alarm function, the miss rate ν with respect to τ (Molchan, 1990, 1991; Molchan and Keilis-Borok, 2008). Then, we have $G = (1 - \nu)/\tau$. An important advantage of the Molchan diagram is that we can visualize instantaneously the so-called Molchan trajectory (τ, ν) and its derivative, which reflects locally, near a specific alarm-function value, the incremental forecast ability of the alarm-based model with respect to the chosen reference model.

There is actually a growing body of theoretical and observational evidence that suggests a dependency of the early aftershock decay rate on stress (Narteau *et al.*, 2002, 2003, 2005, 2008, 2009; Shebalin, 2004). Based on the hypothesis that the time delay before the onset of the power-law aftershock decay rate decreases as the level of stress increases, the Early Aftershock STatistics (EAST) model is an alarm-based forecast model that uses early aftershock statistics to determine the space–time regions where this time delay is abnormally low (Shebalin *et al.*, 2011). In contrast with epidemic-type forecast models, the EAST model concentrates only on the temporal properties of large magnitude aftershocks ($1.8 \geq M^A$) of small magnitude mainshocks ($2.5 \geq M^M \geq 4.5$) to infer the seismogenic potential of the testing region. This model is being tested in the CSEP California testing center, beginning as of 1 July 2009, and it shows better predictive power than the relative intensity (RI) reference model at a level of significance of 1%. This reference model is commonly used because it is simply obtained by smoothing the location of earthquakes in the past (Kossobokov and Shebalin, 2003; Helmstetter *et al.*, 2006; Molchan and Keilis-Borok, 2008; Zechar and Jordan, 2008).

Method

When compared to a reference model, the probability gain G of an alarm-based model is an integral measure for the space–time region that encompasses all the zones where the alarm-function value exceeds a given threshold. Nevertheless, the alarm-based model is likely to perform differently for various ranges of alarm-function values. Rapid and slow variations of the miss rate ν may be observed. For this reason, it seems natural to introduce a differential probability gain $g^{\text{ref}}_{\text{alarm}}$ to measure for each range of alarm-function value the additional amount of information contained in the alarm-based model.

In a Molchan diagram, this differential probability gain is simply defined as the absolute value of the local slope of the Molchan trajectory. Then, we should have $g^{\text{ref}}_{\text{alarm}} = -\partial\nu/\partial\tau$ for a continuous set of alarm-function values and an infinite number of target earthquakes. In practice, given the small number of large magnitude earthquakes in instrumental catalogs and the heterogeneous nature of the spatial distribution of seismicity, the Molchan trajectory is a steplike function. Consequently, we approximate this trajectory by segments, each of them corresponding to different ranges of alarm-function values. Within each segment $g^{\text{ref}}_{\text{alarm}}$ is constant and equal to

$$g^{\text{ref}}_{\text{alarm}} = -\frac{\Delta\nu}{\Delta\tau}. \tag{1}$$

We consider that the dependency of $g^{\text{ref}}_{\text{alarm}}$ on the alarm-function value is constant over time and we calculate it retrospectively over a long time period. Thus, spatial and temporal variations of the $g^{\text{ref}}_{\text{alarm}}$-value result only from changes in the alarm-function value. For the incremental region associated with a lower range of alarm-function value, $g^{\text{ref}}_{\text{alarm}}$ is the ratio between the event rate predicted by the alarm-based and the reference model in this specific space–time region. Then, the new rate-based model is the product of λ_{ref}, the event rate of the reference model, multiplied by the corresponding differential probability gain:

$$\lambda_{\text{alarm}} = g^{\text{ref}}_{\text{alarm}} \lambda_{\text{ref}}. \tag{2}$$

These two terms vary with the magnitude range of the target earthquakes and from one spatial bin to the next. Both terms may also vary over time: for $g^{\text{ref}}_{\text{alarm}}$, this is because of the local fluctuations of the alarm-function value; for λ_{ref}, it is because we can consider a time-dependent reference model.

An important aspect of this conversion method (equation 2) is that the initial rates of the reference model increase or decrease according to the local $g^{\text{ref}}_{\text{alarm}}$-value. Thus, the resulting rate-based model injects into the reference model the additional knowledge carried by the alarm-based model.

From Alarm- to Rate-Based Forecast Model Using Early Aftershock Statistics

To isolate space–time regions with a relative high level of stress, the EAST forecast model uses the E_a-value, the ratio between the long-term and short-term estimations of $\langle t_g \rangle$ (the geometric mean of elapsed times between mainshocks and early aftershocks within a fixed time window; Shebalin *et al.*, 2011). However, mainshock–aftershock sequences are not uniformly distributed, and this alarm function cannot be defined everywhere at all time steps.

In these cases, the alarm-function value is taken equal to λ_{RI}, the normalized event rate given by the RI reference model (Shebalin *et al.*, 2011). Finally, the single alarm function of the EAST forecast model is

$$A_{E_{a1}} = \begin{cases} E_{a1} = \dfrac{E_a}{\lambda_g} = \dfrac{\langle t_g \rangle_{\mathrm{long}}}{\langle t_g \rangle_{\mathrm{short}} \lambda_g} & \text{if } \langle t_g \rangle_{\mathrm{long}} \text{ and } \langle t_g \rangle_{\mathrm{short}} \text{ are defined,} \\ \lambda_{\mathrm{RI}} & \text{otherwise,} \end{cases} \tag{3}$$

where λ_g is a spatially-smoothed event rate similar to λ_{RI}. λ_{RI} is obtained by uniform smoothing within circles of 12-km radius, while λ_g is obtained from a 2D Gaussian function with a standard deviation of 10 km (Shebalin *et al.*, 2011). This Gaussian filter is chosen to assign a nonzero value to all space–time regions. The prospective CSEP test of the EAST forecast model for California started officially on 1 July 2009.

For California from 1984 to 2008, Figure 1 illustrates how we calculate the function $g^{\mathrm{RI}}_{E_{a1}}$, the differential probability gain of the EAST model with respect to the RI reference model. Figures 1a and 1b show the discretization method of the Molchan trajectory for $3.95 \leq M_{\mathrm{target}} < 4.45$ and $5.95 \leq M_{\mathrm{target}}$, respectively. In each of these figures, we see that, for a given range of alarm-function values, the $g^{\mathrm{RI}}_{E_{a1}}$-value is equal to the local slope of the corresponding section of the Molchan trajectory. The limits of these sections are arbitrary chosen to smooth the Molchan trajectory with a minimum number of segments. Figure 1a–e shows that the $g^{\mathrm{RI}}_{E_{a1}}$-values increases with respect to an increasing M_{target}-value. In addition, from

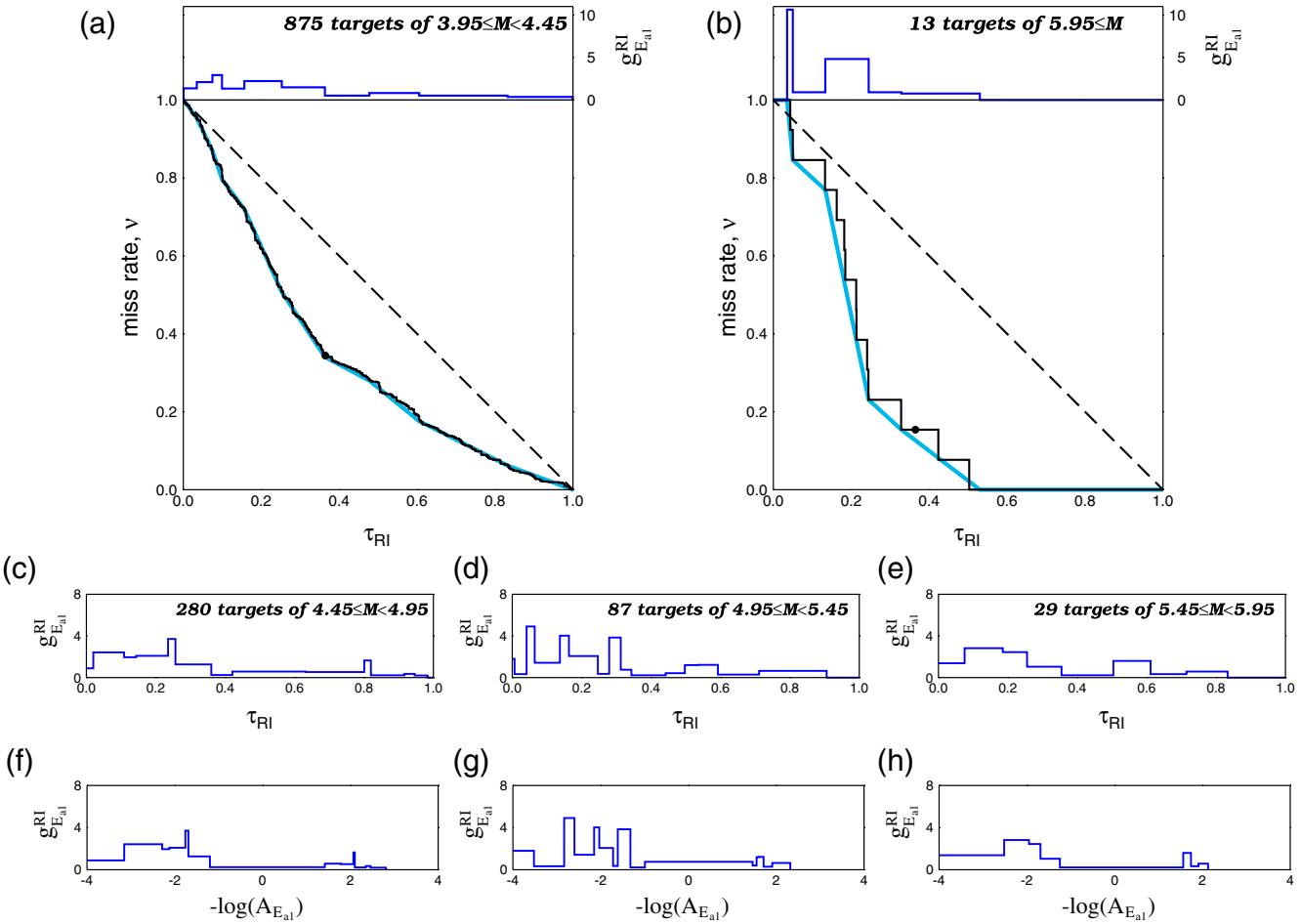

Figure 1. Estimation of the differential probability gains, $g^{\mathrm{RI}}_{E_{a1}}$, of the EAST forecast model with respect to the RI reference model for California from 1984 to 2008. The discretization method of the Molchan trajectories (thin dark lines) for (a) $3.95 \leq M_{\mathrm{target}} < 4.45$ and (b) $5.95 \leq M_{\mathrm{target}}$. The $g^{\mathrm{RI}}_{E_{a1}}$-value is the local slope of the discrete Molchan trajectory (thick light line). Dark points on Molchan trajectories show the limit at which the alarm-function value of the EAST model switches from E_{a1} to λ_{RI} (see equation 3). The $g^{\mathrm{RI}}_{E_{a1}}$-value with respect to τ_{RI} and the alarm-function value $A_{E_{a1}}$ for (c,f) $4.45 \leq M_{\mathrm{target}} < 4.95$, (d,g) $4.95 \leq M_{\mathrm{target}} < 5.45$, and (e,h) $5.45 \leq M_{\mathrm{target}} < 5.95$. The color version of this figure is available only in the electronic edition.

the comparison between Figure 1c–e and Figure 1f–h, we can infer the complex relationship between the alarm-function value and the event rate of the RI reference model in the corresponding region.

Exploiting these differential probability gain functions $g^{\mathrm{RI}}_{E_{a1}}$, we convert the EAST forecast model into a new rate-based model called EAST$_R$. In practice, to derive a rate λ_{RI} from the RI reference model, we need an average number of earthquakes per time bin (three months) and a scaling factor to redistribute these events in all target-earthquake magnitude ranges. Here, for the sake of simplicity, we consider the number of $M \geq 3.95$ earthquakes observed in the time-interval during which the RI reference model has been calculated and a constant slope, $b = 0.96$, of the earthquake-size distribution in California (Knopoff, 2000). Then, according to equation (2), the map of the new rate parameter $\lambda_{E_{a1}}$ of the EAST$_R$ model is simply the local product between λ_{RI} and the corresponding $g^{\mathrm{RI}}_{E_{a1}}$-value.

To present an example of such a conversion from an alarm- to a rate-based model, we use the current alarm function of the EAST forecast model in California (i.e., the three-month period lasting from 1 January to 31 March 2011). For this time period, Figure 2 shows input and output forecast maps of the conversion from EAST to EAST$_R$: input forecasts are the alarm function of the EAST model (Fig. 2a) and the rates of the RI reference model (Fig. 2b); output forecasts are the rate parameter $\lambda_{E_{a1}}$ of the new EAST$_R$ model for $M_{\mathrm{target}} \geq 4$ (Fig. 2c) and $M_{\mathrm{target}} \geq 6$ (Fig. 2d).

Retrospective and Quasi-Prospective Tests

The conversion method can be tested retrospectively from 1984 to 2008 (Fig. 3) but also for the period during which the EAST forecast model has been evaluated in the CSEP California testing center (Fig. 4). This quasi–prospective test covers the six first-three-month forecast periods of the EAST model from 1 July 2009 to 31 December 2010. For this test, we use the CSEP California testing region (Fig. 4a–c) and also a smaller region (Fig. 4d–f) in which the catalogs of early aftershocks are likely to be more complete (see fig. 2 in Shebalin *et al.*, 2011). We use only this smaller region in the retrospective analysis.

In Figures 3 and 4, we perform two types of comparison using Molchan diagrams:

1. We compare the prediction of both the EAST and EAST$_R$ models to the prediction of the RI reference models. The alarm function of the EAST$_R$ model in each space–time region is equal to the cumulative expected rate of target earthquakes on the corresponding magnitude range.
2. We compare the prediction of the EAST model to the prediction of the EAST$_R$ model. Both models change for different magnitude ranges. For the EAST$_R$ model, we use the cumulative expected rate of target earthquakes on the corresponding magnitude range of target earthquakes. When used as the reference model, these rates are normalized by the total cumulative rate for the entire testing region over the full duration of the test. Then, according to a decreasing alarm-function value of the EAST model (i.e., an increasing space–time region), we are able to measure the proportion of events predicted by the EAST$_R$ model in the corresponding region.

For the retrospective test, the prediction of the EAST$_R$ forecast model shows the same performance as the original alarm-based model relative to the prediction of the RI reference model (Fig. 3). For the quasi-prospective tests, all the Molchan trajectories are also similar (Fig. 4). Then, for all time periods, the EAST$_R$ forecast model has better predictive power than the reference model at a level of significance of 1%. In addition, the direct comparison between the original alarm-based model and the obtained rate-based model shows that the EAST and EAST$_R$ models have similar predictive skills (dotted lines in Fig. 4). The only exception is the better performance of the EAST model in the quasi-prospective test for $M_{\mathrm{target}} \geq 3.95$ (Fig. 4d). This difference may be explained by the occurrence of the M 7.2 El Mayor–Cucapah earthquake of 4 April 2010 and the huge proportion of $M \geq 3.95$ aftershocks in the number of target events.

In Table 1, we present the results of standard CSEP likelihood tests for evaluating the forecast of the EAST$_R$ model and compare them to the forecast of the RI reference model (Zechar, Gerstenberger, and Rhoades, 2010). We have not implemented the N-test because the expected number of event is quite stable for the EAST$_R$ model ($\approx$14 per three months for $M \geq 3.95$) and constant for the RI reference model. Similarly, we do not show the results of the M-test as we consider a constant b-value to estimate the event rate of the RI reference model. We see from Table 1 that log-likelihood values in both the L- and S-tests are closer to zero for the EAST$_R$ model than for the RI reference model. This better performance of the EAST$_R$ model is particularly true for two periods, from September to December 2009 and from April to June 2010. Interestingly, the first time period includes a swarm near China Lake, while the second covers the earthquake sequence triggered by the M 7.2 El Mayor–Cucapah earthquake.

Discussion and Conclusions

Our conversion method from alarm- to rate-based forecast model can also be used for alarm-based models, for which the alarm function is a binary variable (alarm, no alarm). The M8, CN, and RTP algorithms mentioned in the Introduction are among them. For these binary forecast models, there is a single point (ν, τ) on the Molchan diagram. Considering our discretization technique, the Molchan trajectory is decomposed in two lines, one for each range of alarm-function values. For the space–time region in which an alarm is issued, we have $g^{\mathrm{ref}}_{\mathrm{alarm}} = G = (1-\nu)/\tau$. Outside these regions, we have $g^{\mathrm{ref}}_{\mathrm{alarm}} = \nu/(1-\tau)$. Then, for a given reference model, as the probability gain of the binary model

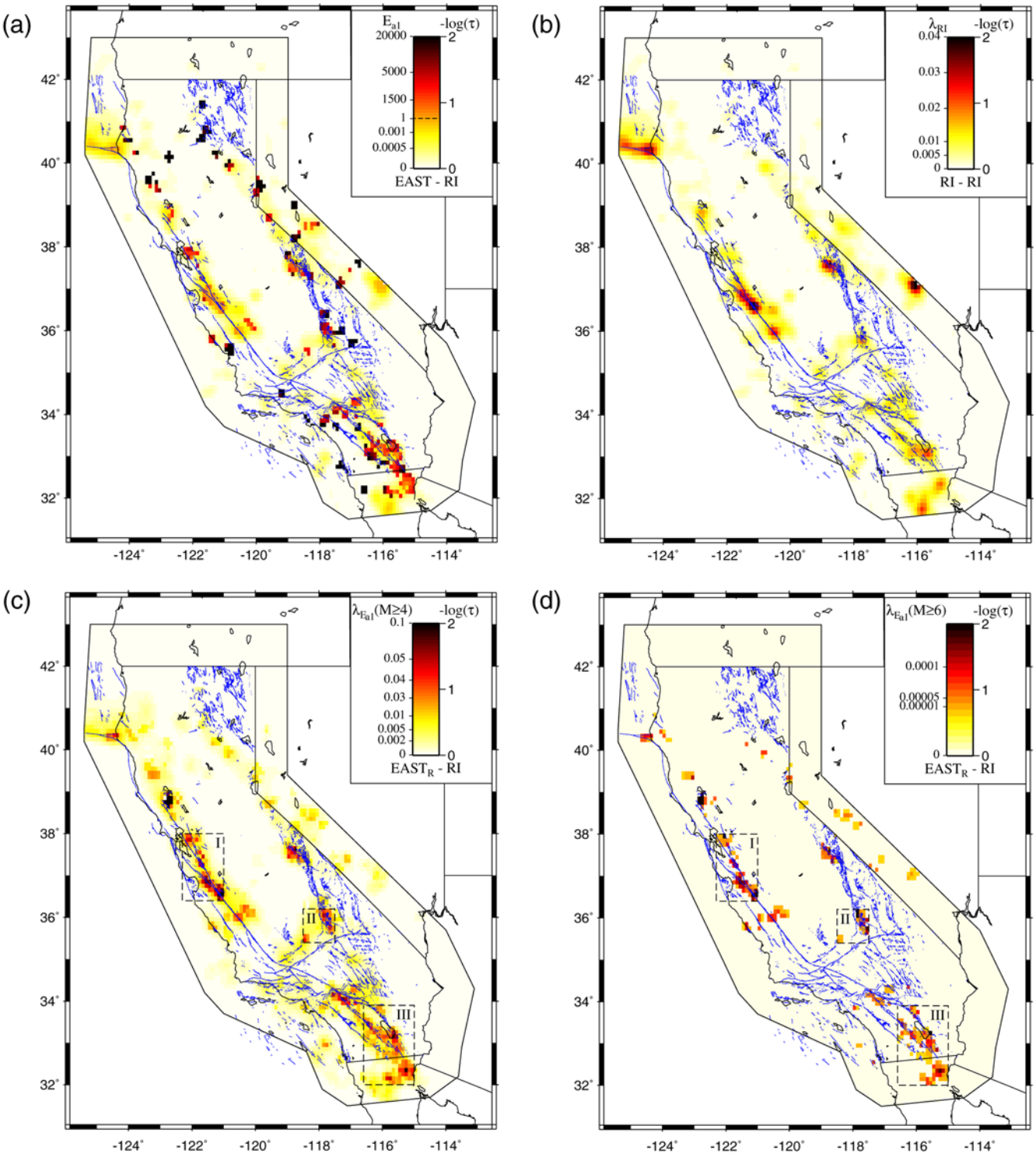

Figure 2. Input and output forecast maps of the conversion from EAST to $EAST_R$ in California from 1 January 2011 to 31 March 2011. Inputs are (a) the alarm-function value of the EAST forecast model and (b) the RI reference model. Output are forecast maps of the rate parameter $\lambda_{E_{a1}}$ of the $EAST_R$ model for (c) $M_{\text{target}} \geq 4$ and (d) $M_{\text{target}} \geq 6$. Color bars are in units of the logarithm of τ, the normalized event rate predicted by the RI reference model in space–time regions in which the alarm-function value of the tested model is larger than a given threshold value. For the $EAST_R$ and RI reference models, the alarm function is the sum of the expected rates over all magnitude bins. The relationship between the τ_{RI}-value and the alarm-function value is shown using the color bars. Note that logarithmic scale is used for better contrast. In (c) and (d), dashed boxes indicate three areas of high $\lambda_{E_{a1}}$-values. The color version of this figure is available only in the electronic edition.

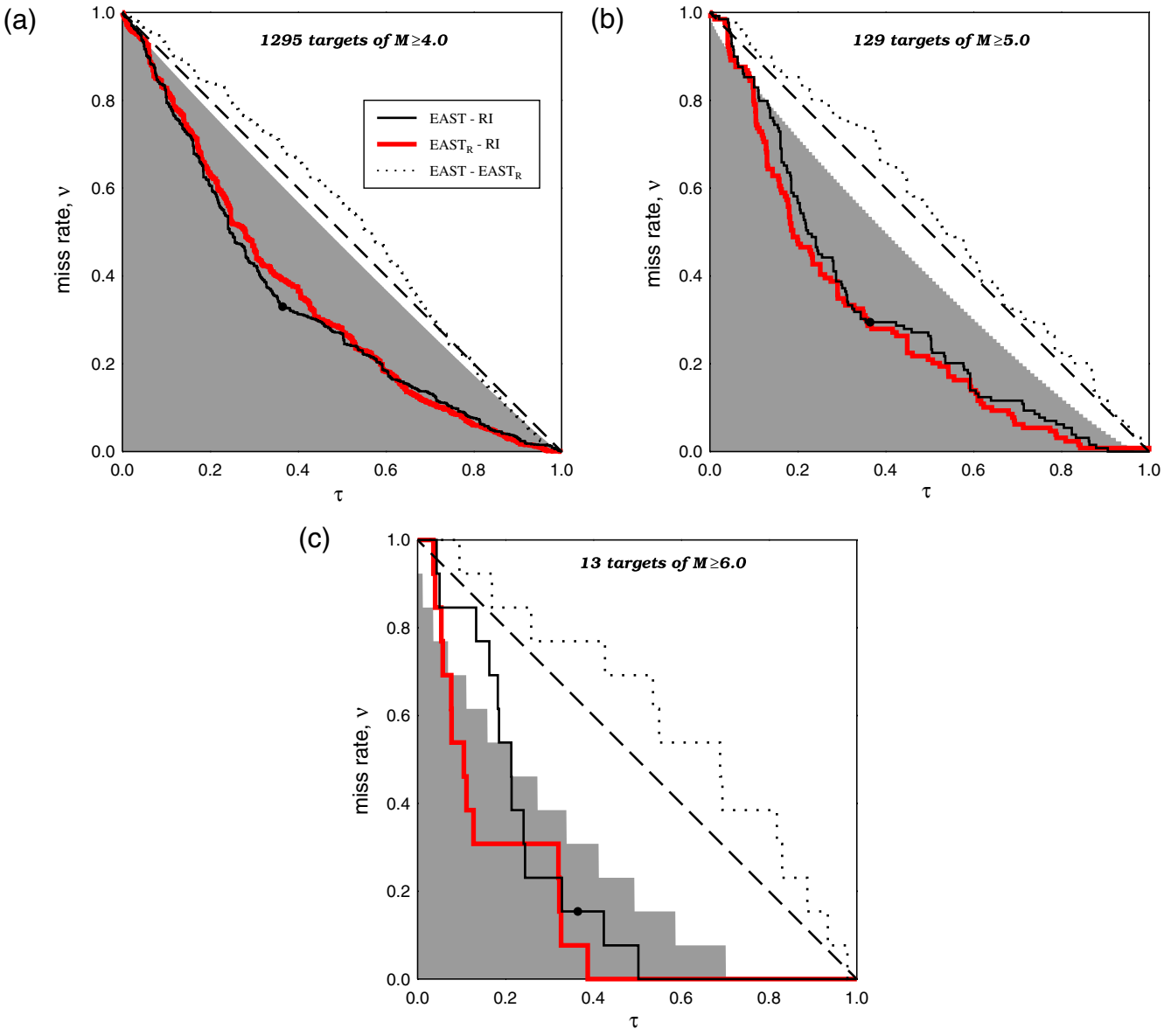

Figure 3. Retrospective evaluation of both the EAST and EAST$_R$ models in California from 1984 to 2008 for (a) $M_{\text{target}} \geq 3.95$, (b) $M_{\text{target}} \geq 4.95$, and (c) $M_{\text{target}} \geq 5.5$. Using Molchan diagrams, we compare the prediction of both the EAST (thin solid lines) and EAST$_R$ models (thick lines) to the prediction of the RI reference model. We also compare the prediction of the EAST model to the prediction of the EAST$_R$ model (dotted lines). The dashed diagonal line corresponds to an unskilled forecast. The shaded area indicates the zone in which the prediction of the tested model outperforms the prediction of the reference model at a level of significance $\alpha = 1\%$. Dark points on Molchan trajectories show the limit at which the alarm-function value of the EAST model switches from E_{a1} to λ_{RI} (see equation 3). The $\lambda_{E_{a1}}$-value of the EAST$_R$ model is equal to the cumulative expected rate of target earthquakes on the corresponding magnitude range. The color version of this figure is available only in the electronic edition.

increases, there is a correspondingly higher contrast of the rates of the converted model within and outside alarms.

Here, we only perform conversion from alarm- to rate-based forecast model using as a reference a stationary rate-based model constructed from a smoothed extrapolation of past seismicity and a constant b-value. Any other rate-based models may be used, for example to take into account spatial and temporal variations of the b-value. Moreover, for large regions we could also improve the model by considering that the dependency of the differential probability gain $g_{\text{alarm}}^{\text{ref}}$ on the alarm-function value varies from one point to another. By construction, the only restriction actually results from the hypothesis that $g_{\text{alarm}}^{\text{ref}}$ is constant over time. This is certainly a strong assumption given the stochastic nature of seismicity, especially for large magnitude earthquakes for which the recurrence time may be larger than the time coverage of the catalogs. Nevertheless, our predictions and their stability should improve as we increase the period of time over which the differential probability gain are estimated. In addition, because our method can also be used to successively

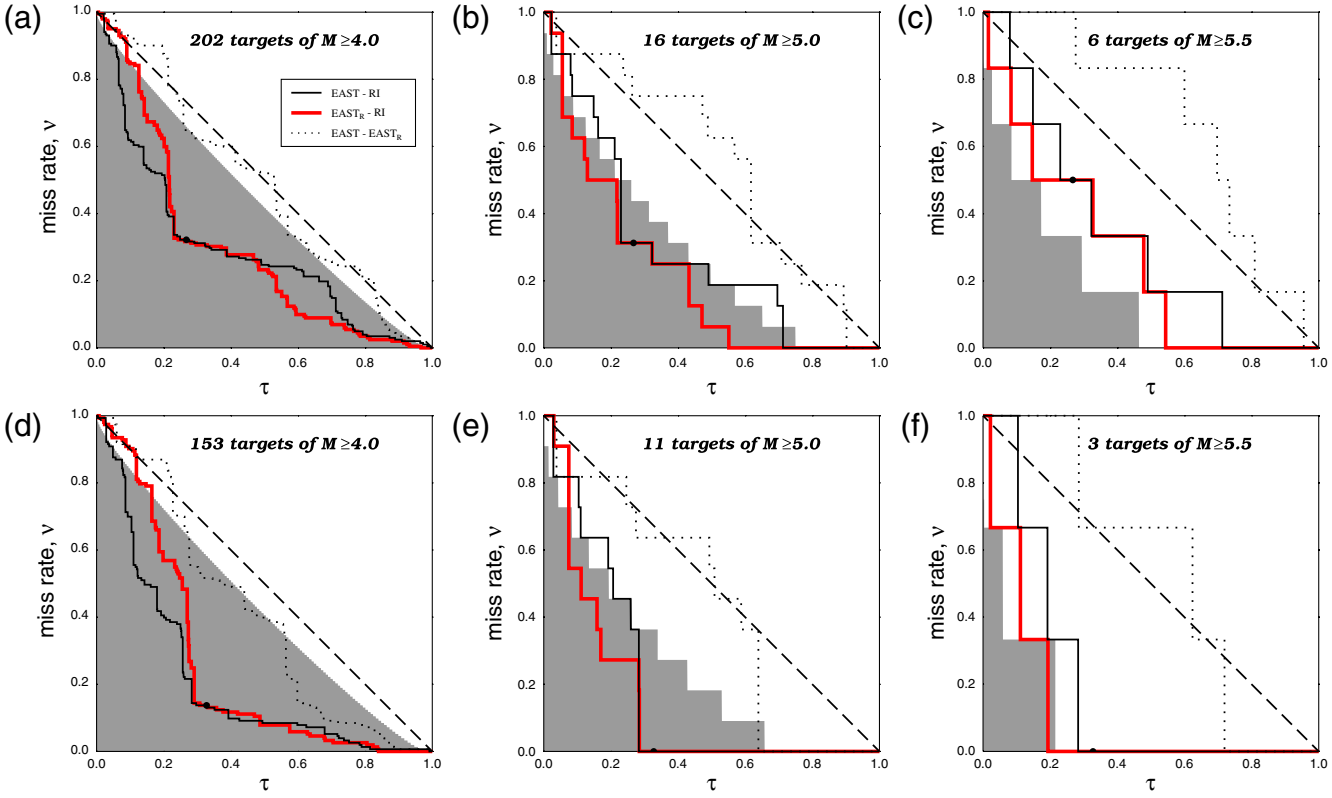

Figure 4. Quasi–prospective evaluation of both the EAST and EAST$_R$ models in California from 1 July 2009 to 31 December 2010 for (a, d) $M_{\text{target}} \geq 3.95$, (b,e) $M_{\text{target}} \geq 4.95$, and (c,f) $M_{\text{target}} \geq 5.5$. Parts (a–c) are for the CSEP California testing region. Parts (d–f) are for the smaller region used in the retrospective test of the EAST forecast model (Shebalin *et al.*, 2011). Using Molchan diagrams, we compare the prediction of both the EAST (thin solid lines) and EAST$_R$ models (thick lines) to the prediction of the RI reference model. We also compare the prediction of the EAST model to the prediction of the EAST$_R$ model (dotted lines). The dashed diagonal line corresponds to an unskilled forecast. The shaded area indicates the zone in which the prediction of the tested model outperforms the prediction of the reference model at a level of significance $\alpha = 1\%$. Dark points on Molchan trajectories show the limit at which the alarm-function value of the EAST model switches from E_{a1} to λ_{RI} (see equation 3). The E_{a1}-value of the EAST$_R$ model is equal to the cumulative expected rate of target earthquakes on the corresponding magnitude range. The color version of this figure is available only in the electronic edition.

combine different models (as described later in this paper), we may introduce a stronger time dependence by taking into account a time-dependent reference model as input to a next iteration.

The prediction of the EAST$_R$ and EAST models show similar performance with respect to the RI reference model both in retrospective and quasi—prospective tests, despite different spatial distributions of their alarm functions (see Fig. 2a in comparison with 2c,d). For all target-earthquake magnitude ranges, the EAST$_R$ models have larger clusters of high alarm-function value that coincide with areas where the rate of the RI reference model are high. Over long testing times, this may improve the forecast skill of the EAST$_R$ model with respect to the EAST model.

Table 1
L- and *S*-Test Results for the Forecasts of the EAST$_R$ and RI Reference Models*

Period	*L*-Test		*S*-Test		N_{target}
	EAST$_R$	RI	EAST$_R$	RI	
Jul.–Aug. 2009	−34.95	−38.13	−19.27	−20.90	3
Sep.–Dec. 2009	−153.18	−167.78	−112.00	−127.29	19
Jan.–Mar. 2010	−178.57	−181.16	−121.28	−122.96	22
Apr.–Jun. 2010	−957.49	−978.11	−573.23	−620.13	129
Jul.–Aug. 2010	−142.68	−144.12	−102.77	−103.94	17
Sep.–Dec. 2010	−104.60	−105.49	−76.47	−77.57	12

*N_{target} is the number of $M \geq 3.95$ earthquakes during the three-month forecast periods.

A general problem for operational forecast is the low magnitude of the predicted event rate in rate-based models (Jordan and Jones, 2010). Evaluating these rates in large clusters may be an appropriate solution for this problem, at least from the point of view of time prediction. For example, let us count the cumulative expected rate of $M \geq 6$ earthquakes in the three clusters of high $\lambda_{E_{a1}}$-value enclosed by boxes in Figure 2c. We obtain cumulative rates of 0.045, 0.014, and 0.038 in boxes I, II, and III respectively. Although these values are higher than the corresponding cumulative rates given by the RI reference model (i.e., 0.039, 0.005, and 0.018, respectively), they remain quite small. Indeed, for a short-term operative forecast, an expected rate of 0.05 seems to be required (Jordan and Jones, 2010). However, for a medium-term forecast, a probability of 0.5 to have an earthquake over a given time period is a reasonable goal. To obtain such a probability, the expected rate of a homogeneous Poisson process should be equal to $-\ln(1-0.5) = 0.69$. Considering the cumulative rates of the three clusters, we conclude that, in California, a time step of three months is too small for an intermediate-forecast of $M \geq 6$ events using the EAST_R model. A time step of two years would be more appropriate. A similar analysis suggests a time step of at least six months for $M_{\text{target}} = 5$. Finally, a time step of three months seems appropriate for $M_{\text{target}} = 4$, even if we consider smaller clusters.

Our conversion method from alarm- to rate-based forecast model can be considered as a more general technique to combine the predictive skills of different types of forecast models. First, this is because all types of forecast models can be easily converted into an alarm-based form. Second, and more importantly, this is because the differential probability gain is a local measure of the additional amount of information provided by an alarm-based model with respect to a rate-based model. Then, multiplying these initial rates by the local differential probability gain is a strategy to amalgamate this knowledge into a reference model. By definition, it makes sense only when the predictions of the alarm-based model outperforms the prediction of the reference model. In this case, this technique may be used several times to combine the advantage of different types of forecast models and seismic hazard maps.

Using the concept of the differential probability gain, we infer that a larger predicted event rate may be achieved from pairwise combinations of the best forecast models. Hence, research efforts can now focus on two directions of study:

1. The conversion from alarm-based to rate-based forecast models in order to estimate the probability of occurrence of an earthquake within the space–time region occupied by alarms.
2. The combination of different forecast models into a single one in order to reach sufficiently high predicted event rates.

Then, we conclude that these studies may provide new opportunities for operational forecast purposes within the framework of CSEP testing centers.

Data and Resources

The prospective test of the EAST model is carried out in the framework of Collaboratory for the Study of Earthquake Predictability (CSEP; http://www.cseptesting.org/, last accessed September 2011). The Advanced National Seismic System (ANSS; http://quake.geo.berkeley.edu/cnss/catalog-search.html, last accessed September 2011) earthquake catalog was searched. Most of the plots were made using the Generic Mapping Tools, version 4.2.1 (http://gmt.soest.hawaii.edu, last accessed September 2011; Wessel and Smith, 1998).

Acknowledgments

The paper has been improved by the constructive comments of J. Zechar and I. Zaliapin. The work was partially supported by the Russian Foundation for Basic Research (RFBR) grant 11-05-00530-a.

References

Aki, K. (1996). Scale dependence in earthquake phenomena and its relevance to earthquake prediction, *Proc. Natl. Acad. Sci. Unit. States Am.* **93,** 3740–3747.

Gerstenberger, M. C., L. M. Jones, and S. Wiemer (2007). Short-term aftershock probabilities: Case studies in California, *Seismol. Res. Lett.* **78,** 66–77.

Gusev, A. (1976). Indicator earthquakes and prediction, in *Seismicity and Deep Structure of Siberia and Far East* V. I. Keilis-Borok and A. A. Soloviev, Nauka, Novosibirsk, Russia, 241–247 (in Russian).

Helmstetter, A., Y. Y. Kagan, and D. D. Jackson (2006). Comparison of short-term and time-independent earthquake forecast models for southern California, *Bull. Seismol. Soc. Am.* **96,** 90–106.

Jordan, T. H. (2006). Earthquake predictability, brick by brick, *Seismol. Res. Lett.* **77,** 3–6.

Jordan, T., and L. Jones (2010). Operational earthquake forecasting: Some thoughts on why and how, *Seismol. Res. Lett.* **81,** 571–574.

Keilis-Borok, V., and V. Kossobokov (1990). Premonitory activation of earthquake flow-algorithm M8, *Phys. Earth Planet. In.* **61,** 73–83.

Keilis-Borok, V., and I. Rotwain (1990). Diagnosis of time of increased probability of strong earthquakes in different regions of the world-algorithm CN, *Phys. Earth Planet. In.* **61,** 57–72.

Knopoff, L. (2000). The magnitude distribution of declustered earthquakes in southern California, *Proc. Natl. Acad. Sci. Unit. States Am.* **97,** 11,880–11,884.

Kossobokov, V., and P. Shebalin (2003). Earthquake prediction, chapter 4 in *Nonlinear Dynamics of the Lithosphere and Earthquake Prediction*, V. I. Keilis-Borok and A. A. Soloviev, Springer-Verlag, Berlin-Heidelberg, 141–205.

Molchan, G. (1990). Strategies in strong earthquake prediction, *Phys. Earth Planet. In.* **61,** 84–98.

Molchan, G. (1991). Structure of optimal strategies in earthquake prediction, *Tectonophysics.* **193,** 267–276.

Molchan, G., and V. Keilis-Borok (2008). Earthquake prediction: Probabilistic aspect, *Geophys. J. Int.* **173,** 1012–1017.

Narteau, C., S. Byrdina, P. Shebalin, and D. Schorlemmer (2009). Common dependence on stress for the two fundamental laws of statistical seismology, *Nature* **462,** 642–645, doi 10.1038/nature08553.

Narteau, C., P. Shebalin, and M. Holschneider (2002). Temporal limits of the power law aftershock decay rate, *J. Geophys. Res.* **107,** doi 10.1029/2002JB001868.

Narteau, C., P. Shebalin, and M. Holschneider (2005). Onset of power law aftershock decay rates in southern California, *Geophys. Res. Lett.* **32,** doi 10.1029/2005GL023951.

Narteau, C., P. Shebalin, and M. Holschneider (2008). Loading rates in California inferred from aftershocks, *Nonlinear Process. Geophys.* **15,** 245–263.

Narteau, C., P. Shebalin, G. Zöller, S. Hainzl, and M. Holschneider (2003). Emergence of a band-limited power law in the aftershock decay rate of a slider-block model of seismicity, *Geophys. Res. Lett.* **30,** doi 10.1029/2003GL017110.

Peresan, A., G. Costa, and G. Panza (1999). Seismotectonic model and CN earthquake prediction in italy, *Pure Appl. Geophys.* **154,** 281–306.

Rhoades, D. A., and M. C. Gerstenberger (2009). Mixture models for improved short-term earthquake forecasting, *Bull. Seismol. Soc. Am.* **154,** no. 2A, 636–646, doi 10.1785/0120080063.

Romashkova, L., and V. Kossobokov (2004). Intermediate-term earthquake prediction based on spatially stable clusters of alarms, *Dokl. Earth Sci.* **398,** 947–949.

Shebalin, P. (2004). Aftershocks as indicators of the state of stress in a fault system, *Dokl. Earth Sci.* **398,** 978–982.

Shebalin, P., V. Keilis-Borok, I. Zaliapin, S. Uyeda, T. Nagao, and N. Tsybin (2004). Advance short-term prediction of the large Tokachi-Oki earthquake, September 25, 2003, $m = 8.1$-a case history, *Earth Planets Space* **56,** 715–724.

Shebalin, P., C. Narteau, M. Holschneider, and D. Schorlemmer (2011). Short-term earthquake forecasting using early aftershock statistics, *Bull. Seimol. Soc. Am.* **101,** no. 1, 297–312, doi 10.1785/0120100119

Wessel, P., and W. Smith (1998). New, improved version of Generic Mapping Tools released, *Eos Trans. AGU* **79,** no. 47, 579.

Zechar, J. (2010). Evaluating earthquake predictions and earthquake forecasts: A guide for students and new researchers, *Community Online Resource for Statistical Seismicity Analysis* 1–26, doi 10.5078/corssa-77337879.

Zechar, J., and T. Jordan (2008). Testing alarm-based earthquake predictions, *Geophys. J. Int.* **172,** 715–724, doi 10.1111/j.1365-246X.2007.03676.x.

Zechar, J., and T. Jordan (2010). The area skill score statistic for evaluating earthquake predictability experiments, *Pure Appl. Geophys.* **167,** 893–906.

Zechar, J. D., M. C. Gerstenberger, and D. A. Rhoades (2010). Likelihood-based tests for evaluating space-rate-magnitude earthquake forecasts, *Bull. Seismol. Soc. Am.* **100,** no. 3, 1184–1195, doi 10.1785/0120090192.

Zechar, J. D., T. H. Jordan, D. Schorlemmer, and M. Liukis (2007). Comparison of two earthquake predictability evaluation approaches, Molchan error trajectory and likelihood, *Seismol. Res. Lett.* **78,** 250.

Zechar, J., D. Schorlemmer, M. Liukis, J. Yu, F. Euchner, P. J. Maechling, and T. H. Jordan (2010). The Collaboratory for the Study of Earthquake Predictability perspective on computational earthquake science, *Concurrency Comput. Pract. Ex.* **22,** 1836–1847.

International Institute of Earthquake Prediction Theory and Mathematical Geophysics
Moscow, 84/32 Profsouznaya
Moscow 117997
Russia
(P.S.)

Equipe de Dynamique des Fluides Géologiques
Institut de Physique du Globe de Paris
Sorbonne Paris Cité, Univ. Paris Diderot
UMR 7154 Centre National de la Recherche Scientifique (CNRS)
1 rue Jussieu
75238 Paris, Cedex 05
France
(C.N.)

Institutes of Applied and Industrial Mathematics
Universtität Potsdam
POB 601553
14115 Potsdam
Germany
(M.H.)

Manuscript received 28 April 2011